

# Late afterglows of GW/GRB 170817A

Houri Ziaeepour<sup>1,2\*</sup>

<sup>1</sup>*Institut UTINAM, CNRS UMR 6213, Observatoire de Besançon, Université de Franche Comté, 41 bis ave. de l’Observatoire, BP 1615, 25010 Besançon, France*

<sup>2</sup>*Mullard Space Science Laboratory, Holmbury St Mary, Dorking, Surrey RH5 6NT, UK*

Accepted XXX. Received YYY; in original form ZZZ

## ABSTRACT

The gamma-ray burst that followed the first detection of gravitational waves from the merger of a Binary Neutron Stars (BNS) and its low energy counterparts were in many respects unusual. In a previous work we used a phenomenological formulation of relativistic shocks and synchrotron emission to analyse the prompt gamma-ray emission of GW/GRB 170817A. We showed that it was most probably intrinsically faint due to the old age of the progenitor neutron stars and their reduced magnetic field. Here we use the same model to analyse late afterglows of this event. We find that a collision between a mildly relativistic outflow from the merger, also called the cocoon, with the circumburst material can explain observations if synchrotron self-absorption of radio emission and local extinction of optical/IR photons are taken into account. These processes are overlooked in the literature. The outflow is presumably the remnant of polar dynamical ejecta during the collision of the neutron stars and at the time of its encounter with circumburst material could have been still magnetized. The most plausible origin for optical extinction is an old faint star cluster surrounding the BNS, which additionally had helped its formation and merger. Such an environment is consistent with our conclusions about evolution and properties of the progenitor neutron stars and may evade present observational constraints. Alternatively, if the synchrotron emission was produced internally through collisions of density shells in the cocoon, the extinction has occurred inside the outflow itself rather than externally. Without a significant extinction of optical/IR emission an additional source of X-ray would be necessary. Decay of medium and heavy nuclides produced by the kilonova, including r-processes, and recombination of electrons may be the missing source of X-ray excess.

**Key words:** gamma-ray burst, gravitational wave, binary neutron star, merger

## 1 INTRODUCTION

The afterglow of GRB 170817A associated to the Gravitational Wave (GW) event GW 170817 is the only short GRB with very long follow up in a broad band of energies, from X-ray to radio. The motivation for studying these faint emissions is not only investigating the fate of a Binary Neutron Star (BNS) merger remnant, but also understanding the origin of unusual faintness of the prompt gamma-ray emission of GRB 170817A and peculiar behaviour of its afterglows, namely its early faintness and late brightening<sup>1</sup>. Explanations suggested in the literature include: off axis observation of both prompt and afterglow of an otherwise ordinary short GRB (Kathirgamaraju, *et al.* 2018; Lazzati, *et al.* 2017; Troja, *et al.* 2017, 2018; Murguia-Berthier, *et al.* 2017); prompt gamma-ray emission from breakout of a chocked jet and afterglow from a mildly relativistic structured jet (Lamb & Kobayashi 2017; Lyman, *et al.* 2018) - also called a *cocoon* (De Colle, *et al.* 2017; Piro, *et al.* 2014; Nakar & Sari 2012; Gottlieb, *et al.* 2017; Kasliwal, *et al.* 2017a; Mooley, *et al.* 2017; Nakar, *et al.* 2018); prompt emission from a structured jet and afterglow from a roughly spherical outflow (Meng, *et al.* 2018; Margutti, *et al.* 2018).

Predictions of these models have been only compared with late X-ray and radio afterglows, because no observation in these bands was performed before  $\sim T + 1.6$  days, where  $T$  is the Fermi-GBM (Dingus 1995) trigger time. No counterpart was detected before  $\sim T + 10$  days and  $\sim T + 16$  days in X-ray and radio wavelengths, respectively. The earliest observations in optical/IR began at the same time as in X-ray and radio and leaded to the detection of a counterpart. However, emissions in optical/IR bands are believed to be dominated by a kilonova originated from the ejection of hot low velocity material from the disk/torus of the merger (Arcav, *et al.* 2017; Berger, *et al.* 2013; Smartt, *et al.* 2017; Covino, *et al.* 2017; Cowperthwaite, *et al.* 2017; Kasen, *et al.* 2017; Nicholl, *et al.* 2017; Metzger, *et al.* 2018) and not from the GRB producing jet. Nonetheless, a contribution from the polar outflow, which generates a relativistic jet and a GRB, may be necessary to explain these observations (Arcav, *et al.* 2017; Smartt, *et al.* 2017). We remind that most works on the unusual properties of GRB 170817A do not compare their models with the prompt emission data obtained by the Fermi-GRB (Goldstein, *et al.* 2017) and the Integral-IBIS (Savchenko, *et al.* 2017) instruments, and only their consistency with the data is discussed.

\* Email: houriziaeepour@gmail.com

<sup>1</sup> In this work by *early afterglow* we mean emissions in X-ray and lower energy bands from  $\gtrsim 70$  sec - the average slew delay of the Neil Gehrels Swift Observatory (Gehrels, *et al.* 2004) - up to  $\mathcal{O}(1) \times 10^5$  sec, i.e. a couple of days after gamma-ray trigger. This is the time interval in which the afterglow of most short GRBs detected by the Swift have been observed. Usually no later attempt is made to detect afterglows of GRBs without an X-ray counterpart in this period and GRB 170817A is an exception.

In a previous work (Ziaeepour 2018) we used a phenomenological formulation of relativistic shocks and their synchrotron/self-Compton emission (Ziaeepour 2009; Ziaeepour & Gardner 2011) to model in detail light curves and spectrum of the prompt gamma-ray emission of GRB 170817A. It shows that the most plausible Lorentz factor for the relativistic jet of this burst is  $\Gamma \sim 100$ . This is much higher than values suggested in the literature, but few folds less than what is predicted for more typical short GRBs, for instance GRB 130603B (Melandri, *et al.* 2013), which was also associated to a kilonova (Berger, *et al.* 2013; Tanvir, *et al.* 2013). Moreover, density and extent of the jet were more than an order of magnitude less than GRB 130603B. Using results of BNS merger simulations, we concluded that probable reasons behind the weak relativistic jet in GW 170817 BNS merger event were: the old age of neutron star progenitors and their reduced magnetic field, thereby less energy for acceleration and formation of a relativistic jet; the closeness of their masses to each other; and the evolutionary history and gravitational disturbance of the BNS orbit due to its encounter and gravitational disturbance by other stars, probably in the dense environment of a cluster, which misaligned spin direction of the neutron stars, leading to a reduced polar ejecta during their collision.

To complete our analysis of GW/GRB 170817A electromagnetic data in this work we present simulations of late afterglow observations according to the same phenomenological model as one used for the modelling of its prompt emission. We first give a very brief summary of the model and its parameters in Sec. 2. Methodology of modelling, initial conditions, and assumptions are discussed in Sec. 3. Results of the simulations are presented in Sec. 4. Interpretation of the results are discussed in Sec. 5, and outlines in Sec. 6. In Appendix A we calculate synchrotron self-absorption index for the phenomenological shock model of (Ziaeepour 2009; Ziaeepour & Gardner 2011). Appendix B summarizes phenomenological expressions used for modelling the width of synchrotron emitting region.

## 2 MODEL

The phenomenological model of (Ziaeepour 2009; Ziaeepour & Gardner 2011) assumes that GRB emissions are produced by synchrotron/self-Compton processes in a dynamically active region in the head front of shocks between density shells inside a relativistic cylindrical jet for prompt and with surrounding material for afterglows in lower energies. In addition to the magnetic field generated by Fermi processes in the active region an external magnetic field precessing with respect to the jet axis may contribute in the production of synchrotron emission. An essential aspect of this model,

which distinguishes it from other phenomenological GRB formulations, is the evolution of parameters with time. Moreover, simulation of each burst consists of a few time intervals - *regimes* - each corresponding to an evolution rule (model) for phenomenological quantities such as: fraction of kinetic energy transferred to fields and its variation; variation of the thickness of synchrotron/self-Compton emitting *active* region; etc. Division of simulated bursts to these intervals allows to change parameters and phenomenological evolution rules which are kept constant during one time interval. As we will explain in more details in the next section, this simplified formulation of shocks is more suitable for prompt and early afterglow emissions, which presumably are generated by a fast and compact ejecta. If, as suggested in the literature (Kasliwal, *et al.* 2017a; Gottlieb, *et al.* 2017; Mooley, *et al.* 2017; Hotokezaka, *et al.* 2018; D’Avanzo, *et al.* 2018) and we give more arguments in its favour in the next section, the observed late afterglows are produced by a continuous flow with varying spatiotemporal characteristics, then strictly speaking the model of (Ziaeepour 2009; Ziaeepour & Gardner 2011) cannot be applied. However, for the time being a better phenomenological formulation is not available and analysis in the literature are also based on models which simply estimate asymptotic behaviour of quantities through fitting of a phenomenological analytical expression. At least in the model of (Ziaeepour 2009; Ziaeepour & Gardner 2011) the evolution of flow and its emission are calculated rigorously from first principles rather than phenomenology. We will discuss uncertainties related to shortcomings of the model in the next section.

Table 1 summarizes parameters of the model. Despite their long list, simulations of typical long and short GRBs in (Ziaeepour & Gardner 2011) show that the range of values which lead to realistic bursts are fairly restricted. Evidently, the range of some parameters for simulation of prompt and afterglow are very different. In particular, we assume that in external shocks, the ISM or surrounding material is at rest with respect to a far observer at the same redshift as the central object. Therefore, external shocks have always a bulk Lorentz factor  $\Gamma = 1$ .

### 3 LATE AFTERGLOW OF GW/GRB 170817A

It is unlikely that the observed electromagnetic emissions from GW/GRB 170817A event at  $\gtrsim T + 10$  days can be due to the remnant of the relativistic jet which generated the observed prompt gamma-ray. The early afterglows of short GRBs are usually observable for few days, see e.g. (Kann 2012) because their flux declines very quickly in all bands. Therefore, as other authors concluded (Mooley, *et al.* 2017; Margutti, *et al.* 2018; D’Avanzo, *et al.* 2018), at  $\gtrsim T + 10$  days the relativistic jet of

**Table 1.** Parameters of the phenomenological relativistic shock model

Model (mod.)	Model for evolution of active region with distance from central engine; See Appendix B and (Ziaeepour 2009; Ziaeepour & Gardner 2011) for more details.
$r_0$ (cm)	Initial distance of shock front from central engine.
$\Delta r_0$	Initial (or final, depending on the model) thickness of active region.
$p$	Slope of power-law spectrum for accelerated electrons; See eq. (3.8) of (Ziaeepour & Gardner 2011).
$p_1, p_2$	Slopes of double power-law spectrum for accelerated electrons; See eq. (3.14) of (Ziaeepour & Gardner 2011).
$\gamma_{cut}$	Cut-off Lorentz factor in power-law with exponential cutoff spectrum for accelerated electrons; See eq. (3.11) of (Ziaeepour & Gardner 2011).
$\gamma'_0$	Initial Lorentz factor of fast shell with respect to slow shell.
$\delta$	Index in the model defined in eq. (3.29) of (Ziaeepour & Gardner 2011).
$Y_e$	Electron yield defined as the ratio of electron (or proton) number density to baryon number density.
$\epsilon_e$	Fraction of the kinetic energy of falling baryons of fast shell transferred to leptons in the slow shell (defined in the slow shell frame).
$\alpha_e$	Power index of $\epsilon_e$ as a function of $r$ .
$\epsilon_B$	Fraction of baryons kinetic energy transferred to induced magnetic field in the active region.
$\alpha_B$	Power index of $\epsilon_B$ as a function of $r$ .
$N'$	Baryon number density of slow shell.
$\kappa$	Power-law index for $N'$ dependence on $r'$ .
$n'_c$	Column density of fast shell at $r'_0$ .
$\Gamma$	Lorentz factor of slow shell with respect to far observer.

★ The phenomenological model discussed in (Ziaeepour 2009) and its simulation (Ziaeepour & Gardner 2011) depends only on the combination  $Y_e \epsilon_e$ . For this reason only the value of this combination is given for simulations.

★ The model neglects variation of physical properties along the jet or active region. They only depend on the average distance from center  $r$ , that is  $r - r_0 \propto t - t_0$ .

★ Quantities with prime are defined with respect to rest frame of slow shell, and without prime with respect to central object, which is assumed to be at rest with respect to a far observer. Power indices do not follow this rule.

GRB 170817A, which according to our analysis its kinetic energy, extent, and density were much smaller than typical short GRBs (Ziaeepour 2018), has been already dissipated by interaction with its surrounding material and had no longer a significant contribution in the observed emissions. Therefore, the observed late brightening of GRB 170817A and a few other short (Fong, *et al.* 2013; Oates, *et al.* 2009) and long (Cummings, *et al.* 2006; De Pasquale, *et al.* 2006) GRBs should be due to emission from another component of ejecta and/or other processes. Candidates are: MHD instabilities leading to increase in magnetic energy dissipation (Levinson & Begelman 2013; Bromberg & Tchekhovskoy 2016); external shocks generated by the collision between the ISM or circumburst material and a mildly relativistic thermal cocoon ejected at the same time as the ultra-relativistic component and lagged with respect to the jet (Nakar & Piran 2016; De Colle, *et al.* 2017; Lyman, *et al.* 2018; Hotokezaka, *et al.* 2018); late outflows from a long lasting accretion disk (Murase, *et al.* 2017); fall-back of ejected matter to the central black hole (Li, *et al.* 2018).

The off-axis view of a structured jet predicts late brightening of afterglows (Lazzati, *et al.* 2016, 2017; Margutti, *et al.* 2018; Kathirgamaraju, *et al.* 2018). However, the observed decline of X-ray flux at  $\lesssim T + 134$  days (D’Avanzo, *et al.* 2018) is inconsistent with simulations of off-axis emission (Lazzati,

(*et al.* 2017), which predict a break after a few hundred days. Other simulations, for instance those reported by (Margutti, *et al.* 2018; Gill & Granot 2018) predict earlier break, but cannot discriminate between off-axis and cocoon (structured jet) models (Mooley, *et al.* 2017) and need polarimetry and imaging to discriminate between them (Gill & Granot 2018). Therefore, emission from collision of a mildly relativistic component of the ejected material during merger seems the most plausible origin for the late brightening of afterglows. Indeed, General Relativistic Magneto-Hydro-Dynamic (GRMHD) simulations of BNS merger show poleward mildly relativistic mass ejection (Foucart, *et al.* 2016; Dionysopoulou, *et al.* 2015; Kiuchi, *et al.* 2014). A small fraction of this ejecta is accelerated to ultra-relativistic velocities by the transfer of Poynting energy of the ejecta to kinetic energy (Komissarov, *et al.* 2009; Tchekhovskoy, *et al.* 2008; Bromberg & Tchekhovskoy 2016). The remaining material continues its trajectory and eventually collides with the ISM and/or circum-BNS material at a later time. If this scenario is correct, brightening in other short GRBs with detected afterglow is simply missed due to the lack of sufficiently long observations.

In this work we assume that the late afterglow of GRB 17081A is due to the mildly relativistic remnant of dynamical ejecta during BNS merger, which from now on we call the *cocoon* or simply the *outflow*.

### 3.1 Initial conditions of the cocoon

Before discussing how we have estimated initial conditions for the simulation of late afterglows of GRB 17081A we should remind that in the phenomenological model of (Ziaeepour 2009; Ziaeepour & Gardner 2011) the jet is cylindrical and as long as the line of sight of the observer pass through it and its Lorentz factor is sufficiently high such that  $\sin \theta_j > 1/\gamma'$ , the effect of oblique view is negligible<sup>2</sup>. Additionally, it is proved that for  $\Gamma_j \gg 1$  the contribution of high latitude emission is small (Ziaeepour 2009). This condition is not fully satisfied by the cocoon, which by definition is only mildly relativistic. Nonetheless, even for a cocoon with a Lorentz factor  $\Gamma_c \sim 2$  the value of  $1/\Gamma_c^2 \sim 1/4 \sim 1/2\Gamma_c$ . Considering other theoretical and observational uncertainties in the modelling of the data, this amount of error should be tolerable when the aim is order of magnitude estimation of physical quantities which characterize the outflow and material surrounding the BNS merger.

Initial values of some parameters in Table 2 cannot be arbitrarily selected. For instant, the initial

<sup>2</sup> For external shocks  $\Gamma = 1$ . Thus, relative Lorentz factor of shells is equal to Lorentz factor of the jet  $\Gamma_j$  with respect to a far observer at the same redshift as the source.

distance of the jet front from center when the presumed external shock begins must be consistent with the value of cocoon's  $\beta$  and the time of first detection of electromagnetic signal from cocoon's external shock. For  $\beta = 0.4$  and  $0.8$  corresponding to  $\gamma' \approx 1.2$  and  $2.34$ ,<sup>3</sup> the distance of the ejecta's front  $r_0$  at the beginning of its collision with the ISM/surrounding material at  $\lesssim 10$  days after merger must be  $\approx 10^{16}$  cm and  $2 \times 10^{16}$  cm, respectively.

To estimate physically plausible column density of the cocoon we use the results of GRMHD numerical simulations of BNS merger. The total amount of fast tail (dynamical) ejecta is expected to be  $0.01 - 0.03 M_{\odot}$ , where  $M_{\odot}$  is the solar mass (Arcav, *et al.* 2017; Pian, *et al.* 2017; Smartt, *et al.* 2017). In the case of GW 170817 event a larger ejecta of  $m_{ejecta} \sim 0.03 - 0.05 M_{\odot}$  seems necessary to explain the bright UV/blue emission of kilonova at  $\sim T + 1.6$  days (Smartt, *et al.* 2017). However, a contribution from GRB 170817A afterglow in the early blue peak cannot be ruled out (Arcav, *et al.* 2017), see also the discussion about the early afterglow of this burst in (Ziaeepour 2018). We show later that under some conditions our simulations are consistent with the prediction of GRMHD simulations.

Using the above estimated ejecta mass, the baryon number column density at distance  $r_0 = c\beta t_0$  can be parametrized as:  $n'_c = 0.3 \times 10^{25} \eta A / \beta^2 t_{day}^2$ , where  $\eta \equiv \pi/\theta_c$  and  $A \equiv m_{ejecta}/0.01 M_{\odot}$ . We use the approximate time of the first detection of the X-ray counterpart  $t_0 \sim 10$  days to estimate order of magnitude value of column density  $n'_c$  to be used in our simulations. For instance, for  $\beta = 0.8$ ,  $A = 1$ , and a close to spherical outflow, the column density  $n'_c \sim 4.7 \times 10^{22}$  cm $^{-2}$  and  $r_0 \sim 2 \times 10^{16}$  cm; for  $\beta = 0.4$  the column density increases to  $n'_c \sim 1.9 \times 10^{23}$  cm $^{-2}$  and initial distance decreases to  $r_0 \sim 10^{16}$  cm. The values for distance to the ISM found here correspond to typical distance of terminal shock of material ejected from a star, i.e. where the ISM pressure become dominate over the wind. In the cases of GW 170817 event what we call *circumburst* material would be pre-merger, presumably the remnant of ejected matter during and after the formation of neutron stars and BNS.

We should remind that due to the large parameter space of the model it was not possible to perform a systematic search for the best combination of parameters. This fact must be taken into account when simulations are compared with data. In particular, the values of parameters given in Table 2 should be considered as order of magnitude estimations.

<sup>3</sup> Because we assume that  $\Gamma = 1$ , i.e. the ISM/circumburst material is at rest with respect to a far observer at the same redshift,  $\gamma'$  is the Lorentz factor of jet with respect to observer. Nonetheless, we keep ' for consistency of notation with Table 1.

**Table 2.** Parameter set of simulated models.

%scriptsize

Simul. mod. No.	$\gamma'_0$	$r_0$ (cm)	$\frac{\Delta r_0}{r_0}$	$(\frac{r}{r_0})_{max}$	$p$	$\gamma_{cut}$	$\kappa$	$\delta$	$\epsilon_B$	$\alpha_B$	$\epsilon_e Y_e$	$\alpha_e$	$N'$ (cm $^{-3}$ )	$n'_c$ (cm $^{-2}$ )
	1	$2.3 \times 10^{16}$	$10^{-5}$	1.5	1.8	100	-0.1	0.5	$5 \times 10^{-4}$	-1	0.02	-1	$0.5 \times 10^{22}$	
1	2	-	-	-	10	-	100	-0.4	0.1	-	0	-	0	-
	2	-	-	-	50	-	100	0	0.5	-	1	-	1	-
	2	-	-	-	10	-	100	0.5	1	-	1	-	1	-
2	1	$1.2 \times 10^{16}$	$5 \times 10^{-3}$	1.5	1.8	100	-0.5	1	0.05	-1	0.1	-1	1	$5 \times 10^{23}$
	2	-	-	-	15	-	100	0	0.1	-	0	-	0	-
	2	-	-	-	10	-	100	1	1	-	1	-	1	-
3	1	$1.2 \times 10^{16}$	$10^{-3}$	1.5	1.8	100	-0.5	1	0.05	-1	0.1	-1	1	$5 \times 10^{23}$
	2	-	-	-	10	-	100	0	0.1	-	0	-	0	-
	2	-	-	-	10	-	100	1	1	-	1	-	1	-
4	1	$1.2 \times 10^{16}$	$5 \times 10^{-3}$	1.5	2.1	100	-0.5	1	0.08	-1	0.1	-1	0.08	$5 \times 10^{23}$
	2	-	-	-	10	-	100	0	0.1	-	0	-	0	-
	2	-	-	-	10	-	100	1	1	-	1	-	1	-
5	1	$1.2 \times 5 \times 10^{16}$	$10^{-3}$	1.5	2.5	100	-0.5	1	0.05	-1	0.1	-1	0.5	$5 \times 10^{23}$
	2	-	-	-	10	-	100	0	0.1	-	0	-	0	-
	2	-	-	-	10	-	100	1	1	-	1	-	1	-
6	1	$2.3 \times 10^{16}$	$10^{-3}$	1.5	1.8	100	-0.5	1	0.05	-1	0.02	-1	1.e-1	$5 \times 10^{22}$
	2	-	-	-	10	-	100	0.2	0.1	-	0	-	0	-
	2	-	-	-	10	-	100	1.5	1	-	1	-	1	-
7	1	$1.2 \times 10^{16}$	$5 \times 10^{-3}$	2.5	2.1	100	-0.5	1	0.08	-1	0.1	-1	0.008	$10^{22}$
	2	-	-	-	30	-	100	0	0.1	-	0	-	0	-
	2	-	-	-	20	-	100	1	1	-	1	-	1	-

\* For external shocks of jet with the ISM or circumburst material  $\Gamma = 1$  is assumed. In this case  $\gamma'$  is the Lorentz factor of jet with respect of a far observer at the same redshift.

\* Each data line corresponds to one simulated regime, during which quantities listed here remain constant or evolve dynamically according to fixed rules. A full simulation of a burst usually includes multiple regimes (at least two).

\* Horizontal black lines separate time intervals (regimes) of independent simulations identified by the number shown in the first column.

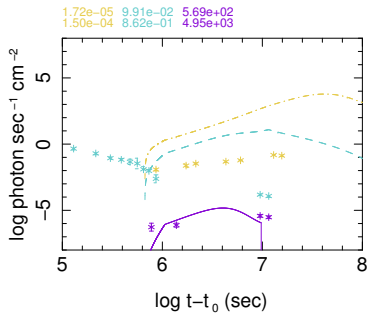
\* A dash as value for a parameter presents one of the following cases: it is irrelevant for the model; it is evolved from its initial value according to an evolution equations described in (Ziaeepour 2009; Ziaeepour & Gardner 2011); or it is kept constant during all regimes.

## 4 SIMULATIONS

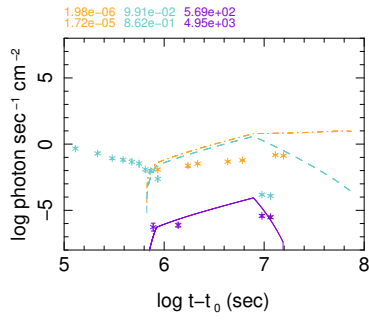
Fig. 1 shows simulations which reproduce well at least one of the 3 energy bands with late observations, namely X-ray, optical/IR and 6 GHz radio band. Parameters of these simulations are shown in Table 2. We remind that only two relatively close in time data points are available in optical/IR band at late times<sup>4</sup>. Earlier data in this band is dominated by the kilonova emission and cannot be used to investigate the origin and properties of late emission, which as we discussed earlier, is presumably produced by another component of ejecta from the BNS merger.

<sup>4</sup> At the time of preparation of this article new observations of GW 170817 counterpart in far-IR at  $\sim T + 264$  days was published Villar, *et al.* (2018). They are not considered in our analysis, partly to avoid further delay in the completion of our work and partly because far-IR emission at the epoch of observations is expected to be dominated by kilonova emission Villar, *et al.* (2018).

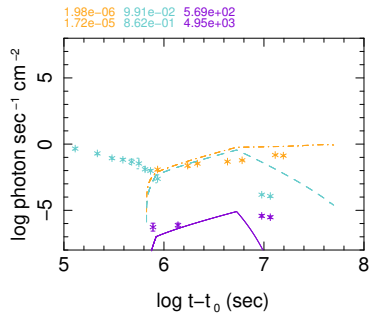
Simul. 1



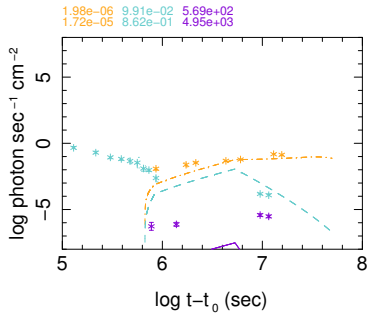
Simul. 2



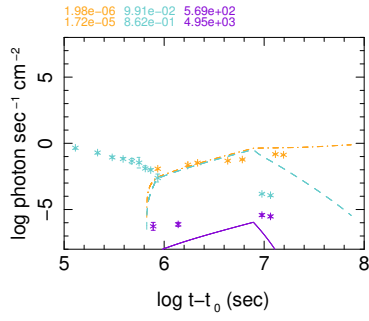
Simul. 3



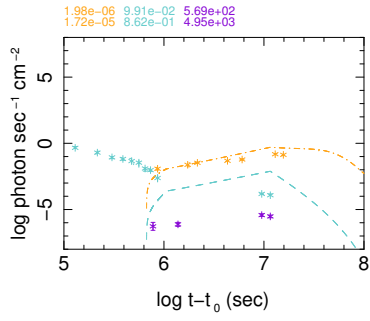
Simul. 4



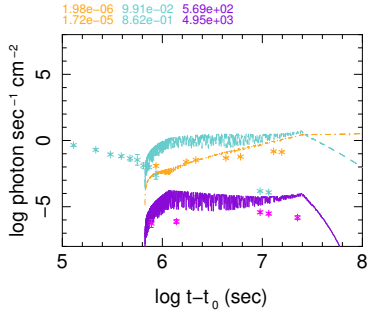
Simul. 5



Simul. 6



Simul. 7



Simul. 8

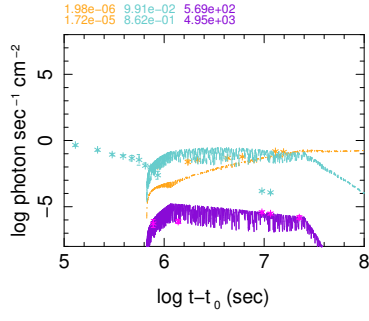


**Figure 1.** X-ray, optical, and radio light curves of simulated models without taking into account synchrotron self-absorption. The energy range for each band is written in the same colour/gray scale as the curve on the top of each plot. Stars present data taken from: (Margutti, *et al.* 2018) (X-ray), (Soares-Santos, *et al.* 2017; Pian, *et al.* 2017; Lyman, *et al.* 2018; D’Avanzo, *et al.* 2018) (optical), (Alexander, *et al.* 2017; Hallinan, *et al.* 2017; Dobie, *et al.* 2018) (radio). Parameters of simulations No. 1 to 6 corresponds to models No. 1 to 6 in Table 2. Simulation No. 7 has the same parameters as simulation No. 4 but include an external magnetic field - presumably a Poynting flow oscillating with a frequency of 0.01 Hz and  $|B| = 5(r/r_0)^{\alpha_m}$  G, where  $\alpha_m = 1, 1, 2$  in the 3 regimes of this simulation. Simulation No. 8 corresponds to model No. 7 in Table 2 and includes an external magnetic field similar to that of simulation No. 7. Note that the plots of the last 2 simulations include X-ray observation by Chandra at  $\sim T + 260$  days (Nynka, *et al.* 2018).

The value of Lorentz factor (or equivalently  $\beta$ ) chosen for these simulations, namely  $\beta = 0.4, 0.8$  correspond to what is used in the literature for simulating late light curves of GW/GRB 170817. However, from Fig. 1 it is clear that none of these simulations can simultaneously fit observations in X-ray, optical/IR and radio bands. Nonetheless, simulations No. 1 and 2 are good fits to X-ray data, simulations No.3 fit X-ray and radio , and simulation No. 4 fits well optical and radio data. A

main difference between simulations which fit X-ray data and those which fit radio data is the higher density of ISM/circum merger material in the former with respect to the latter.

In what concerns X-ray and radio observations these results are not inconsistent with cocoon/fast tail outflow studied in (Hotokezaka, *et al.* 2018) and other attempts to model late afterglows of GW/GRB 170817A Troja, *et al.* (2018); D’Avanzo, *et al.* (2018). The modelling of synchrotron emission in these works is based on the phenomenological formulation of Sari & Piran (1995); Sari, *et al.* (1996). Notably, in the fast tail outflow model of Hotokezaka, *et al.* (2018) it is assumed that the cocoon has a non-uniform energy distribution as a function of  $\Gamma_c \beta_c$ . Then, a phenomenological profile for this distribution is adjusted to fit the data. The shock model of (Ziaeepour 2009) considers collision between a thin shell of material with uniform properties and another shell or circumburst material and cannot simulate continuous variation of outflow/jet density. On the other hand, the evolution of the uniform outflow is calculated more rigorously from first principles. The two classes of our results described above can be interpreted as approximating a continuously varying outflow by a denser front part, which collides with a denser circum-merger material, and a diluted hind part, which collides with the remnant of ISM/circum-merger material after its distortion and spread out by the front of the flow. However, this explanation does not solve the problem of over production of optical and radio emissions by the denser front part of the flow. For instance, an interpolation in time between these models needs zero contribution from the first category of simulations around the time of last X-ray observations to be consistent with optical observations at the same time.

We also considered the effect of a Poynting flow imprinted in the cocoon material. Ejected dynamical material from BNS merger is expected to be highly magnetized and may preserve part of its magnetic energy well after its expansion. Even in the case of main sequence stars such as the Sun a weak magnetic field is detected at upstream of wind termination shock (Burgala, *et al.* 2008).

Simulations No. 7 and 8 in Fig. 1 are examples of the case of a magnetically loaded cocoon. Simulation No. 7 has the same parameter as No. 4 which fits radio and optical data well but has insufficient X-ray. We find that when a magnetic field with initial flux of  $|B| \sim 5$  G is added to this model, both X-ray and optical emissions become much brighter than observations. Simulation No. 8 in 1, corresponding to model No. 7 in Table 2, has more diluted outflow and circum-burst material and the same magnetic field as simulation No. 7. The plots in Fig. Fig. 1 show that its X-ray light curve is consistent with the data. Moreover, the lower column density in this model is better consistent with the estimated value found in Sec 3.1. However, optical emission of the model is too bright and

similar to simulations No. 1 to 3 only in presence of extinction it may be consistent with data. In both examples with an additional magnetic field radio emission remains consistent with observations.

To explain discrepancies between data and simulated optical and radio light curves we must consider two important processes, which are so far overlooked. They are synchrotron self-absorption in radio band and extinction of optical emission by material around the merger and in its environment.

#### 4.1 Absorption

Low energy emissions are absorbed by gas and dust in circumburst material and ISM, and through synchrotron self-absorption process in the shocked region of the cocoon. The main source of absorption for X-ray is neutral atomic gas. The  $H_I$  equivalent column density of the Milky Way  $N_H^{MW}$  in the direction of GW/GRB 170817A is  $7.84 \times 10^{20} \text{ cm}^{-2}$  (Margutti, *et al.* 2017; Troja, *et al.* 2017). Using 0.3-10 keV X-ray data from Chandra, the intrinsic column density in front of the ejecta of GW/GRB 170817A is estimated to be  $\lesssim 3 \times 10^{22} \text{ cm}^{-2} \approx 0.05 \text{ gr/cm}^2$  (Margutti, *et al.* 2017; Troja, *et al.* 2017). It presumably presents material in the local environment of the progenitor BNS and is much smaller than characteristic absorption length of 0.3-10 keV X-ray, which is  $\sim 0.2 \text{ gr/cm}^2$  (Tanabashi, *et al.* 2018). Thus, X-ray absorption is only a few percents (Tanabashi, *et al.* 2018) and negligible with respect to observational and modelling uncertainties.

In astronomical shocks synchrotron self-absorption is significant only in radio band (Rybicki & Lightman 2004). In appendix A we calculate synchrotron self-absorption coefficient in the framework of phenomenological shock model of (Ziaeepour 2009). Plots in Fig. 2 show the effect of synchrotron self-absorption for simulation No. 2 and a phenomenological description for the variation of absorption length with propagation as an exponential or power-law, see Appendix A for more explanation. They confirm that  $\lesssim 6 \text{ GHz}$  radio emission can be completely absorbed if the extension of the induced magnetic field in front of the shocked region is enough long. Indeed, radio emission in both short and long GRBs is only observed at late times and well after the decline of higher energy counterparts. In the case of GW/GRB 170817A the first detection of a counterpart in radio was only a few days after the first detection in X-ray (Hallinan, *et al.* 2017; Pozanenko, *et al.* 2017; Alexander, *et al.* 2017; Mooley, *et al.* 2017; Dobie, *et al.* 2018; Alexander, *et al.* 2018)<sup>5</sup>. However, as it is explained in details in (Ziaeepour 2018) we have most probably missed the early X-ray and optical afterglows. Assuming

<sup>5</sup> Observations in this work was made public after our simulations and are not taken into account in our analysis. Nonetheless, they are consistent with our simulations and their interpretations.

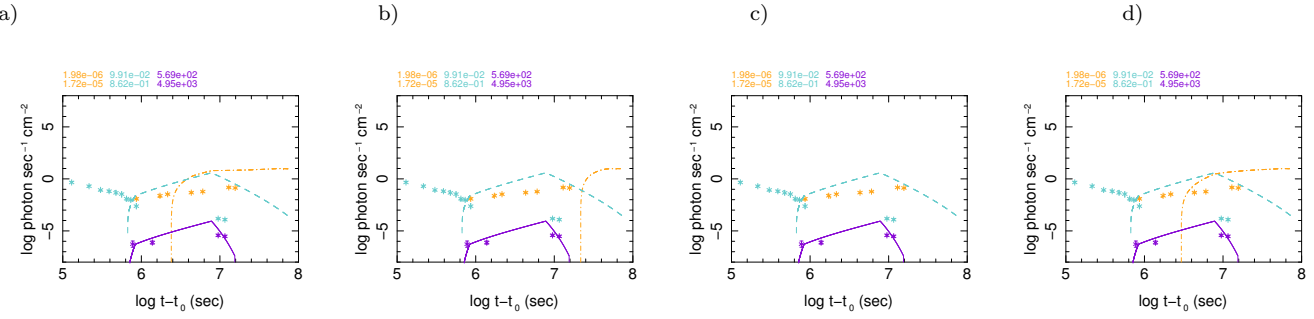


**Figure 2.** Light curves of Model No. 2 with different self-absorption length index  $\alpha$  defined in Appendix A: Exponential dependence on distance and  $\alpha = 1$  (a),  $\alpha = 0.1$  (b), and  $\alpha = 0$  (c); power-law dependence on distance and  $\alpha = 3$  (d). Description of light curves and data is the same as Fig. 1

that the denser front of the cocoon had a long effective length for synchrotron self-absorption, its radio emission was completely extinguished locally and what we observe comes from the weak shocks of the tail of flow presented by simulations No. 4, 5, and 6 in Fig. 1.

Optical and IR bands are mainly affected by dust and electrons in the outer shells of neutral or slightly ionized atomic gas. The extinction in the Milky Way in the direction of GW 170817 is estimated to be only  $A_V \lesssim 0.5$  mag (Coulter, *et al.* 2017). Moreover, due to the very low star formation rate of the host galaxy NGC 4993, the extinction inside the host is believed to be negligible (Covino, *et al.* 2017). Therefore, any further extinction must be local and due to the circum-merger material and environment. As mentioned earlier, X-ray data shows the existence of an equivalent  $N_H \lesssim 3 \times 10^{22} \text{ cm}^{-2}$  column of material in front of the cocoon. If this material were genuinely hydrogen, it had negligible effect on the optical/IR emission. However, in the environment of old collapsed stars a large fraction of this material should consist of heavier elements such as  $O$ ,  $C$ ,  $Fe$ ,  $Si$ , etc. (Güver & Özel 2009). They can significantly affect low energy photons if they are not fully ionized. Indeed, measurements of equivalent column density  $N_H$  and extinction  $A_V$  in supernovae remnants show a linear relation between  $\log N_H$  and  $A_V$ , see e.g. (Reina & Tarenghi 1973; Gorenstein 1975; Predehl & Schmitt 1995). A recent calibration of this relation in SNRs (Güver & Özel 2009) estimates this relation as  $N_H = (2.1 \pm 0.09) \times 10^{21} A_V \text{ (cm}^{-2}\text{)}$ . Using this equation, we find that for  $N_H \lesssim 3 \times 10^{22} \text{ cm}^{-2}$  the amount of extinction in visible band is  $A_V \lesssim 10 \text{ mag} \sim 4 \text{ dex}$ . This amount of extinction can make optical light curve of simulations No. 2, 3, and 8 fully consistent with the data.

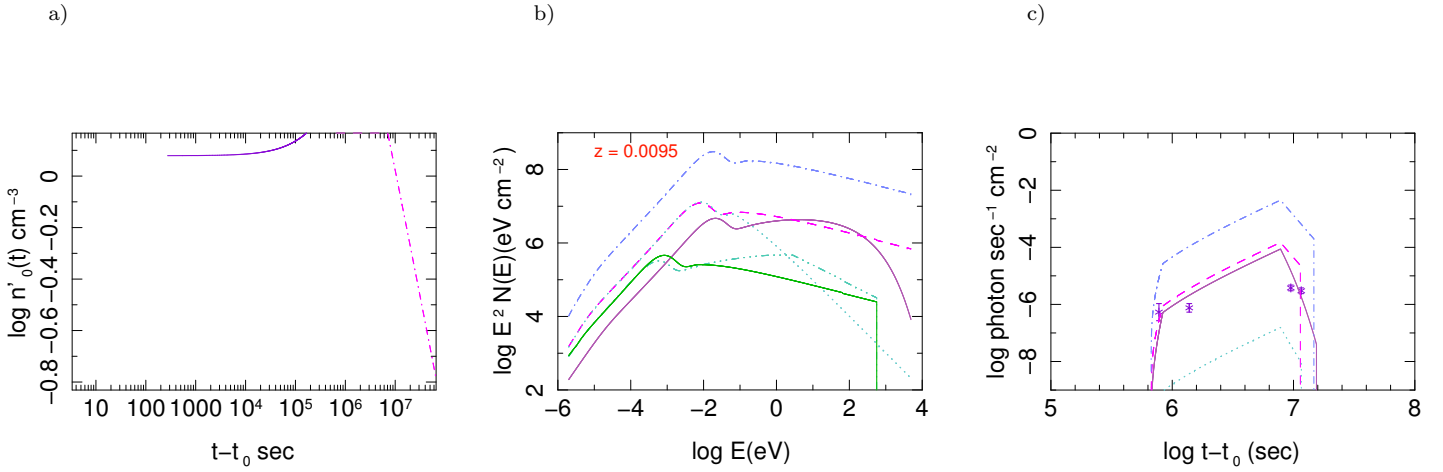


**Figure 3.** a) Profile of the material sheath around the BNS merger. b) Spectra of simulation No. 2 (dark continuous) and several of its variants with broken power-law spectrum for electrons:  $p_2 = 2.5$ ,  $n'_0 = 1 \text{ cm}^{-3}$  and  $\Gamma = 3$  (dashed); the same as the previous with  $n'_0 = 5 \text{ cm}^{-3}$  (dash-dot);  $p_2 = 2.5$  and  $n'_c = 5 \times 10^{22} \text{ cm}^{-2}$  (dash-dot-dot);  $p_2 = 3$  (dash-dot-dot-dot); and  $p_2 = 4$ ,  $n'_0 = 1 \text{ cm}^{-3}$  and  $\Gamma = 3$  (light continuous). c) X-ray light curves of models in b). The last two models in b) do not have significant emission in this band due to a noticeable break in their spectra at  $\sim 0.5 \text{ keV}$  because the simulation code was not able to follow the evolution of rapidly fainting X-ray.

## 5 DISCUSSION

To generate a light curve consistent with observations we assumed a density profile for the ISM/circumburst matter, see Fig. 3-a. It evolves with the distance from central object according to a power-law with index  $\kappa$  (see Table 1). Its value for each model can be found in Table 2. This phenomenological model allows to determine the profile of circumburst matter dynamically. It was presumably formed during the lifetime of the progenitor neutron stars (Slane 2017) and its compression in front of the outflow was responsible for generating a density discontinuity and a shock. Simulations shown in Fig. 1 demonstrate that the density of this sheath at the initial position of the shock front in the simulations must be at least few fold larger than average ISM density of the host galaxy reported in the literature, namely  $\sim 0.04 \text{ cm}^{-3}$  based on the absence of significant neutral hydrogen in the host (Hallinan, *et al.* 2017). For lower densities the X-ray flux would be too small.

Irrespective of the results of our simulations, interpretation of multi-band observations as synchrotron or thermal emission would be very difficult if no optical/IR extinction was occurred. Fig. 4 shows the distribution of energy flux density at  $\sim T + 110$  days, for which data in all three bands X-ray, optical/IR and radio is available. We remind that this distribution is independent of viewing angle and geometry of emitting surface, which are not well understood and are subject to debate and controversies. It depends only on the emission mechanism. The observed distribution significantly deviates from a typical synchrotron and thermal spectra (shown in Fig. 4), or a more realistic nonlinear + synchrotron + thermal spectrum (Burgess, *et al.* 2017; Warren, *et al.* 2017). It is not possible either

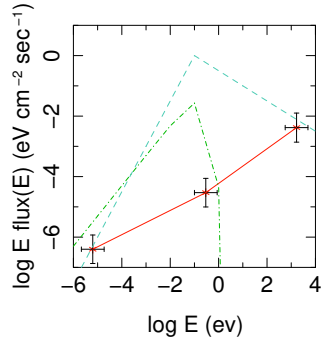


**Figure 4.** Energy flux distribution of GW/GRB 170817A at  $\sim T + 110$  days. Bars on the data points present the width of corresponding energy band rather than measurement errors, which are much smaller. A typical synchrotron spectrum (dashed) is sketched by its asymptotic behaviour with theoretical slope of  $3/2$  at low energy wing and a chosen slope of  $-1/2$  for high energy wing. Its peak is adjusted to a value close to simulated spectra shown in Fig. 3-b. A thermal spectrum with the same temperature as peak energy of the synchrotron spectrum is also shown (dash-dot). The continuous line connecting data points is drawn as guide for comparison with other curves.

to assume that all the three energy bands fall on the low energy wing of the spectrum, because its positive slope is much flatter than  $3/2$  of synchrotron emission. Moreover, if this assumption were true, the source had to be observable in higher energy bands.

A large extinction of optical photons is consistent with the fact that optical afterglow of the majority of short bursts are not detected, most probably due to the intrinsic absorption (Kopac, *et al.* 2012; Roming, *et al.* 2009). Moreover, the upper limit on the  $N_H$  obtained from X-ray observations and its associated extinction are consistent with those of globular clusters, see e.g. (Froebrich & Rowles 2010). In addition, the probability of formation and merger of BNS is higher in star clusters than in the field. However, multiband observations of NGC 4993 seems to be inconsistent with the presence of a globular or young star cluster with a total mass larger than a few thousands solar masses (Levan, *et al.* 2017). Thus, the results of the modelling of late afterglow and conclusions from observations of the host galaxy and surroundings of the progenitor BNS do not seem fully consistent with each. An excess of X-ray emission from kilonova remains a possibility, but it needs quantitative estimation of its significance. On the other hand, both theoretical and interpretation of observations are in large extent uncertain.

For the reasons explained earlier the phenomenological formalism of (Ziaeepour 2009; Ziaeepour & Gardner 2011) is more suitable for modelling prompt emissions from an ultra relativistic jet than a mildly relativistic outflow with continuously varying properties. Thus, uncertainties in simulated models may be significant. Nonetheless, general aspects of their spectra seem correct, see Fig. 3-b for some examples (and corresponding X-ray light curves in Fig. 3-c). Therefore, it is unlikely that the difficulty of simulations to explain multi-band observations without considering absorption of

low energy photons be simply due to theoretical shortcomings of the model. Indeed, Fig. 3-b shows that for  $\Gamma \lesssim 3$ , ISM/circumburst density of  $\mathcal{O}(1)$ , and column density of flow as estimated in Sec. 3.1, the optical/IR band falls in the high energy wing of the spectrum. The only way to reduce the amount of energy emitted in optical band seems to be increasing the peak energy to energies much higher than optical band. This is consistent with necessity of an additional source of X-ray discussed above. This cannot be achieved without much higher Lorentz factor and densities and is in contradiction with what is expected from a mildly relativistic outflow Nakar, *et al.* (2018) and a low density ISM/circumburst material, as observations of the host galaxy shows (Hallinan, *et al.* 2017). On the other hand, a star cluster dominated by old faint and/or compact stars as the local environment of GW 170817 event may evade multi-wavelength observations and constraint of (Levan, *et al.* 2017). For instance, the absolute magnitude limit of  $M_V > -6.7$  concluded for any star cluster from observations of (Levan, *et al.* 2017) is much brighter than the old faint star cluster Segue 3 (Fadely, *et al.* 2011; Hughes, *et al.* 2017) which has an absolute magnitude of  $M \sim 0$  or even a star cluster  $\sim 400$  fold brighter than Segue 3.

Alternatively, the late afterglow may be the result of multiple collisions between density shells in a mildly relativistic outflow rather than one collision. In this case emissions from shocks occurring closer to the center must pass through the outflow and will be subject to absorption. This scenario is similar to internal shocks in a relativistic jet, but here the flow is only mildly relativistic and shells will need much more time to catch with each other and collide. Our simulations show that in such a model shocks should have properties similar to model No. 3 if only a few shell collisions occurred or model No. 5 if many collisions had taken place. The column densities of these models are consistent with the estimation of  $N_H$  in short GRBs (Kopac, *et al.* 2012). It is also enough to provide the necessity extinction.

A significant contribution from kilonova may solve the problem if the emission is in X-ray. A thermal emission in X-ray from a very hot ejected disk at  $\gtrsim T + 100$  seems unlikely. In fact observation of the counterpart in far IR at  $\sim T + 264$  days shows that at this epoch the kilonova is cooled and its dominant emission is in far IR (Villar, *et al.* 2018). On the other hand, X-ray from decay of nuclides produced in the kilonova and/or recombination of electrons in the ejected disk remain a possibility. Indeed, hundreds of electronic excitation lines and isotopes with half-life of  $\mathcal{O}(100)$  exists, including those related to nuclides produced through r-process Chu, *et al.* (1999). This alternative solution needs a quantitative investigation, which must include calculation of nuclides yield in the kilonova and evolution of their ionization state.

## 6 OUTLINES

In conclusion, shocks generated by the collision of a mildly relativistic outflow - a cocoon - with a sheath of material surrounding the merger or density layers inside the outflow can explain brightening and other characteristics of X-ray, optical/IR, and radio counterparts of GW/GRB 170817A. We suggested two scenarios for the generation of these afterglows.

In the first scenario synchrotron self-absorption and extinction of optical emission in the environment of the source are necessary to explain late multi-band observations. The most probable origin of the external extinction, which may be additionally responsible for the faintness of undetected early afterglow of the GRB 170817A, is the presence of an old star cluster surrounding the progenitor BNS. This conclusion is consistent with larger probability of the formation of BNS and their merger in star clusters than in low density regions of galaxies, and conclusions of (Ziaeepour 2018) from the analysis of prompt gamma-ray emission.

In the second scenario multiple shocks generated by collision density shells inside the same outflow provide both the emission and reduction of optical emission with respect to X-ray that we find necessary for explaining observations.

An excess of X-ray - most probably from decay of nuclides and/or recombination of electrons in the kilonova - rather than extinction of optical emission is another possibility, that must be considered and quantified.

## APPENDIX A: SYNCHROTRON SELF-ABSORPTION

Reduction of photon flux of a source due to absorption during propagation of photons in matter is a Possinian process and can be formulated as:

$$\frac{dI_\nu}{d\ell} = \alpha_\nu I_\nu \quad (\text{A1})$$

where  $I_\nu$  is intensity at frequency (energy)  $\nu$  and  $\ell$  is distance propagated in an absorbing matter. For synchrotron self-absorption the absorption coefficient  $\alpha_\nu$  can be related to distribution of accelerated electrons (Rybicki & Lightman 2004):

$$\alpha_\omega = \frac{\pi}{2\omega} \int_{\gamma_e}^{\infty} d\gamma_e P(\omega, \gamma_e) \gamma_e^2 \frac{\partial}{\partial \gamma_e} \left( \frac{n'_e(\gamma_e)}{\gamma_e^2} \right) \quad (\text{A2})$$

where  $\omega = E/\hbar$  is photon mode for a photon of energy  $E$ ;  $\gamma_e$  is Lorentz factor of accelerated electrons;  $n'_e(\gamma_e)$  is number density of electrons with Lorentz factor  $\gamma_e$ ; and  $P(\omega, \gamma_e) \equiv dP/\omega d\omega$  is differential synchrotron power density for mode  $\omega$ .

Using the phenomenological expression of  $P(\omega, \gamma_e)$  obtained in (Ziaeepour 2009), the absorption coefficient  $\alpha_\omega$  can be written as:

$$\alpha_\omega = \frac{\sqrt{3}e^2}{\omega\gamma_m^2} \int_1^\infty d\eta F(\eta) \left[ \int_{\omega/(\omega_m\eta)}^\infty d\zeta K_{5/3}(\zeta) + \dots \right], \quad F(\eta) \equiv \frac{\partial}{\partial\eta} \left( n'_e(\eta) \right) \quad (\text{A3})$$

where  $K_\nu$  is the second modified Bessel function of order  $\nu$  and dots mean higher order subdominant terms which depend on the geometry of the emitting surface. They are neglected in our simulations. This is a good approximation for the prompt emission, in which due to the large Lorentz factor of jet, the effective opening angle visible to a far observer is small and emission is highly beamed. For the late after the effect of high latitude emission can be significant and should be added to other uncertainties of the model. In particular, high latitude emission increases the total duration of afterglow for a given detection threshold. Nonetheless, even for a Lorentz factor as small as 2 the visible opening angle is  $30^\circ$  and delay for arrival of photons from high latitudes would be  $\sim 13\%$  of the time necessary for light to traverse a distance equal to the radius of emission surface. For an initial distance of  $\mathcal{O}(1)10^{16}$  cm used in our simulations and the final radius of  $\sim 10$  times larger, the delay is  $\lesssim 10$  days i.e. comparable with the exposure time in the latest observations. Thus, the increase in emission duration due to high latitude emission is of the same order as uncertainty on the observation time and does not have significant impact on comparison models with data.

Equation (A3) shows that the synchrotron self-absorption coefficient depends on  $\eta \equiv \gamma'_e/\gamma'_c$ ,  $\omega'_c \equiv \frac{3e\gamma_e^2 B'_\perp}{2cm_e}$ , and  $\omega_m = \omega_c|_{\gamma_e=\gamma_m}$  where  $\gamma_m$  is the minimum Lorentz factor of accelerated electrons. The second integral has an approximate analytical expression:

$$\int_{\omega/(\omega_m\eta)}^\infty d\zeta K_{5/3}(\zeta) \approx 2K_{2/3}(\omega/(\omega_m\eta)) \quad (\text{A4})$$

We use this approximate expression in our simulations.

The total amount of synchrotron self-absorption is obtained from integrating eq. (A1). It depends on the geometric extension of magnetic field in the shock front  $D_{sy}$ . In our simulations we assume that this length is proportional to synchrotron characteristic time (Rybicki & Lightman 2004) and reduces exponentially or according to a power-law with propagation of shock front, i.e.  $D_{sy}(r) = ct_{sy}(r)f(r/r_0)$  where  $t_{sy}(r) = 3c\pi\gamma_m^3(r)/\omega'_c(r)$  is the synchrotron characteristic time for electrons with minimum energy;  $c$  is the speed of light; and we consider either  $f(r/r_0) = \exp(-\alpha r/r_0)$  or  $f(r/r_0) = (r/r_0)^\alpha$ .

## APPENDIX B: EVOLUTION MODELS OF ACTIVE REGION

In the phenomenological model of (Ziaeepour 2009) the evolution of  $\Delta r'(r')$  cannot be determined from first principles. For this reason we consider the following phenomenological models:

$$\Delta r' = \Delta r'_0 \left( \frac{\gamma'_0 \beta'}{\beta'_0 \gamma'} \right)^\tau \Theta(r' - r'_0) \quad \text{dynamical model, Model = 0} \quad (\text{B1})$$

$$\Delta r' = \Delta r'_\infty \left[ 1 - \left( \frac{r'}{r'_0} \right)^{-\delta} \right] \Theta(r' - r'_0) \quad \text{Steady state model, Model = 1} \quad (\text{B2})$$

$$\Delta r' = \Delta r'_0 \left( \frac{r'}{r'_0} \right)^{-\delta} \Theta(r' - r'_0) \quad \text{Power-law model, Model = 2} \quad (\text{B3})$$

$$\Delta r' = \Delta r'_\infty \left[ 1 - \exp\left(-\frac{\delta(r' - r'_0)}{r'_0}\right) \right] \Theta(r' - r'_0) \quad \text{Exponential model, Model = 3} \quad (\text{B4})$$

$$\Delta r' = \Delta r'_0 \exp\left(-\delta \frac{r'}{r'_0}\right) \Theta(r' - r'_0) \quad \text{Exponential decay model, Model = 4} \quad (\text{B5})$$

The initial width  $\Delta r'(r'_0)$  in Model = 1 & 3 is zero. Therefore, they are suitable for description of initial formation of an active region in internal or external shocks. Other models are suitable for describing more moderate growth or decline of the active region. In Table 2 the column *mod.* indicates which evolution rule is used in a simulation regime - as defined in the foot notes of this table - using model number given in B1-B5.

## REFERENCES

Alexander, K.D., Berger, E., Fong, W., Williams, P.K.G., Guidorzi, C., Margutti, R., Metzger, B.D., Annis, J., *et al.*, 2017, *ApJ.Lett.*, **848**, L21 [[arXiv:1710.05457](https://arxiv.org/abs/1710.05457)].

Alexander, K.D., Margutti, R., Blanchard, P.K., Fong, W., Berger, E., Hajela, A., Eftekhari, T., Chornock, R., *et al.*, (2018) [[arXiv:1805.02870](https://arxiv.org/abs/1805.02870)].

Arcavi, I., Hosseinzadeh, G., Howell, D.A., McCully, C., Poznanski, D., Kasen, D., Barnes, J., Zaltzman, M., Vasylyev, S., Maoz, D., Valenti, S., 2017, *Nature*, **551**, 64 [[arXiv:1710.05843](https://arxiv.org/abs/1710.05843)].

Levinson, A., Begelman, M.C., 2013, *ApJ.*, **764**, 148 [[arXiv:1209.5261](https://arxiv.org/abs/1209.5261)].

Berger, E., Fong, W., Chornock, R., 2013, *ApJ.Lett.*, **774**, L23 [[arXiv:1306.3960](https://arxiv.org/abs/1306.3960)].

Bromberg, O., Tchekhovskoy, A., 2016, *MNRAS*, **456**, 1739 [[arXiv:1508.02721](https://arxiv.org/abs/1508.02721)].

Burgala, L.F., Ness, N.F., Acuna, M.H., Lepping, R.P., Connerney, J.E.P., Richardson, J.D., 2008, *Nature*, **454**, 75.

Burgess, J.M., Preece, R.D., Connaughton, V., Briggs, M.S., Goldstein, A., Bhat, P.N., Greiner, J., Gruber, D., *et al.*, 2014, *ApJ.*, **784**, 17 [hrefhttps://arxiv.org/abs/1304.4628](https://arxiv.org/abs/1304.4628) [[arXiv:1304.4628](https://arxiv.org/abs/1304.4628)].

Chu, S.Y.F., Ekström, L.P., Firestone, R.B., “The Lund/LBNL Nuclear Data Search”, <http://nucleardata.nuclear.lu.se/toi/>.

Church, R.P., Levan, A.J., Davies, M.B., Tanvir, N., in proceedings of “GRBs as probes: from the progenitor’s environment to the high redshift Universe”, Como, Italy, May 2011, [[arXiv:1110.4209](https://arxiv.org/abs/1110.4209)].

Covino, S., Wiersema, K., Z.Fan, Y., Toma, K., B.Higgins, A., Melandri, A., D’Avanzo, P., G.Mundell, C., *et al.*, 2017, *Nature Astro.*, **1**, 791 [[arXiv:1710.05849](https://arxiv.org/abs/1710.05849)].

Coulter, D.A., Foley, R.J., Kilpatrick, C.D., Drout, M.R., Piro, A.L., Shappee, B.J., Siebert, M.R., Simon, J.D., *et al.*, 2017, *Science*, **358**, 1556 [[arXiv:1710.05452](https://arxiv.org/abs/1710.05452)].

Cowperthwaite, P.S., Berger, E., Villar, V.A., Metzger, B.D., Nicholl, M., Chornock, R., Blanchard, P.K., Fong, W., *et al.*, 2017, *ApJ.Lett.*, **848**, 17 [[arXiv:1710.05840](#)].

Cummings, J.R., Barthelmy, S.D., Gronwall, C., Holland, S.T., Kennea, J.A., Marshall, F.E., Palmer, D.M., Perri, M., (2006) *GCN Circ.* **5301**.

De Colle, F., Lu, W., Kumar, P., Ramirez-Ruiz, E., Smoot, G., (2017) [[arXiv:1701.05198](#)].

D'Avanzo, P., Campana, S., Ghisellini, G., Melandri, A., Bernardini, M.G., Covino, S., D'Elia, V., Nava, L., *et al.*, 2018, *A&A*, **613**, L1 [[arXiv:1801.06164](#)].

De Pasquale, M., Barthelmy, S.D., Campana, S., Cummings, J.R., Godet, O., Guidorzi, C., Hill, J.E., Holland, S.T., Kennea, J.A., *et al.*, (2006) *GCN Circ.* **5409**

Dingus B.L., 1995, *Space Sci.*, **231**, 187

Dionysopoulou, K., Alic, D., Rezzolla, L., 2015, *Phys. Rev. D*, **92**, 084064 [[arXiv:1502.02021](#)].

Dobie, D., Kaplan, D.L., Murphy, T., Lenc, E., Mooley, K.P., Lynch, C., Corsi, A., Frail, D., Kasliwal, M., Hallinan, G., 2018, *ApJ.*, **858**, L15 [[arXiv:1803.06853](#)].

Fadely, R., Willman, B., Geha, M., Walsh, S., Munoz, R.R., Jerjen, H., Vargas, L.C., Da Costa, G.S., 2011, *Astron. J.*, **142**, 88 [[arXiv:1107.3151](#)].

Fong, W.F., Berger, E., Metzger, B.D., Margutti, R., Chornock, R., Migliori, G., Foley, R.J., Zauderer, B.A., *et al.*, 2013, *ApJ.*, **780**, 118 [[arXiv:1309.7479](#)].

Foucart, F., Desai, D., Brege, W., Duez, M.D., Kasen, D., Hemberger, D.A., Kidder, L.E., Pfeiffer, H.P., Scheel, M.A., 2017, *Class.Quant.Grav.*, **34**, 044002 [[arXiv:1611.01159](#)].

Froebrich, D., Rowles, J., 2010, *MNRAS*, **406**, 1350 [[arXiv:1004.0117](#)].

Gehrels, N., Chincarini, G., Giommi, P., Mason, K.O., Nousek, J.A., Wells, A.A., White, N.E., Barthelmy, S.D., *et al.*, 2004, *ApJ.*, **611**, 1005 [astro-ph/0405233](#).

Gill, R., Granot, J., 2018, *MNRAS*, **sty1214**, [[arXiv:1803.05892](#)].

Goldstein, A., Veres, P., Burns, E., Briggs, M.S., Hamburg, R., Kocevski, D., Wilson-Hodge, C.A., Preece, R.D., 2017, *ApJ.Lett.*, **848**, L14 [[arXiv:1710.05446](#)].

Gorenstein, P., 1975, *ApJ.*, **198**, 95.

Gottlieb, O., Nakar, E., Piran, T., Hotokezaka, K., (2017) [[arXiv:1710.05896](#)].

Güver, T., Özel, F., 2009, *MNRAS*, **400**, 2050 [[arXiv:0903.2057](#)].

Hallinan, G., Corsi, A., P.Mooley, K., Hotokezaka, K., Nakar, E., Kasliwal, M.M., Kaplan, D.L., Frail, D.A., *et al.*, 2017, *Science*, **358**, 1579 [[arXiv:1710.05435](#)].

Hotokezaka, K., Kiuchi, K., Shibata, M., Nakar, E., Piran, T., (2018) [[arXiv:1803.00599](#)].

Hughes, J., Lacy, B., Sakari, C., Wallerstein, G., Evan Davis, C., Schiefelbein, S., Corrin, O., Joudi, H., Le, D., Haynes, R.M., 2017, *Astron. J.*, **154**, 57 [[arXiv:1706.01961](#)].

Kann D.A., 2013, *EAS Publications Series*, **61**, 309 [[arXiv:1212.0040](#)].

Kasen, D., Metzger, B., Barnes, J., Quataert, E., Ramirez-Ruiz, E., 2017, *Nature*, **551**, 80 [[arXiv:1710.05463](#)].

Kasliwal, M.M., Nakar, E., Singer, L.P., Kaplan, D.L., Cook, D.O., Van Sistine, A., Lau, R.M., *et al.*, 2017, *Science*, **358**, 1559 [[arXiv:1710.05436](#)].

Kathirgamaraju, A., Barniol Duran, R., Giannios, D., 2018, *MNRAS*, **473**, L121 [[arXiv:1708.07488](#)].

Kiuchi, K., Kyutoku, K., Sekiguchi, Y., Shibata, M., Wada, T., 2014, *Phys. Rev. D*, **90**, 041502 [[arXiv:1407.2660](#)].

Komissarov, S., Vlahakis, N., Konigl, A., Barkov, M., 2009, *MNRAS*, **394**, 1182 [[arXiv:0811.1467](#)].

Kopac, D., D'Avanzo, P., Melandri, A., Campana, S., Gomboc, A., Japelj, J., Bernardini, M.G., Covino, S., *et al.*, 2012, *MNRAS*, **424**, 2392 [[arXiv:1203.1864](#)].

Lamb, G.P., Kobayashi, S., 2017, *MNRAS*, **472**, 4953 [[arXiv:1706.03000](#)].

Lazzati, D., Deich, A., Morsony, B.J., Workman, J.C., 2017, *MNRAS*, **471**, 1652 [[arXiv:1610.01157](#)].

Lazzati, D., Perna, R., Morsony, B.J., López-Cmara, D., Cantiello, M., Ciolfi, R., Giacomazzo, B., Workman, J.C., (2017) [[arXiv:1712.03237](#)].

Lee, W.H., Ramirez-Ruiz, E., van de Ven, G., 2010, *ApJ.*, **720**, 953 [[arXiv:0909.2884](#)].

Levan, A.J., Lyman, J.D., Tanvir, N.R., Hjorth, J., Mandel, I., Stanway, E.R., Steeghs, D., Fruchter, A.S., Troja, E., *et al.*, 2017, *ApJ.Lett.*, **848**, L12 [[arXiv:1710.05444](#)].

Li, B., Li, L.B., Huang, Y.F., Geng, J.J., Yu, Y.B., Song, L.M., 2018, *ApJ.Lett.*, **859**, L3 [[arXiv:1802.10397](#)].

Lyman, J.D., Lamb, G.P., Levan, A.J., Mandel, I., Tanvir, N.R., Kobayashi, S., Gompertz, B., Hjorth, *et al.*, J., (2017) [[arXiv:1801.02669](#)].

Margutti, R., Berger, E., Fong, W., Guidorzi, C., Alexander, K.D., Metzger, B.D., Blanchard, P.K., Cowperthwaite, P.S., *et al.*, 2017, *ApJ.Lett.*, **848**, L20 [[arXiv:1710.05431](#)].

Margutti, R., Alexander, K.D., Xie, X., Sironi, L., Metzger, B.D., Kathirgammaraju, A., Fong, W., Blanchard, P.K., Berger, *et al.*, E., (2017) [[arXiv:1801.03531](#)].

Melandri, A., Baumgartner, W.H., Burrows, D.N., Cummings, J.R., Gehrels, N., Gronwall, C., Page, K.L., M.Palmer, *et al.*, D., (2013) *GCN Circ.* **14735**.

Meng, Y-Z., Geng, J-J., Zhang, B-B., Wei, J-J., Xiao, D., Liu, L-D., Gao, H., Wu, X-F., *et al.*, 2018, *ApJ.*, **860**, 72 [[arXiv:1801.01410](#)].

Metzger, B.D., Thompson, T.A., Quataert, E., 2018, *ApJ.*, **856**, 101 [[arXiv:1801.04286](#)].

Mooley, K.P., Nakar, E., Hotokezaka, K., Hallinan, G., Corsi, A., Frail, D.A., Horesh, A., Murphy, T., Lenc, E., *et al.*, 2018, *Nature*, **554**, 207 [[arXiv:1711.11573](#)].

Murase, K., Toomey, M.W., Fang, K., Oikonomou, F., Kimura, S.S., Hotokezaka, K., Kashiyama, K., Ioka, K., Meszaros, P., (2017) [[arXiv:1710.10757](#)].

Murguia-Berthier, A., Ramirez-Ruiz, E., Kilpatrick, C.D., Foley, R.J., Kasen, D., Lee, W.H., Piro, A.L., Coulter, D.A., *et al.*, 2017, *ApJ.Lett.*, **848**, L34 [[arXiv:1710.05453](#)].

Nakar, E., Sari, R., 2012, *ApJ.*, **747**, 88 [[arXiv:1106.2556](#)].

Nakar, E., Piran, T., 2016, *ApJ.*, **834**, 28 [[arXiv:1610.05362](#)].

Nakar, E., Gottlieb, O., Piran, T., Kasliwal, M.M., Hallinan G., (2018) [[arXiv:1803.07595](#)].

Nicholl, M., Berger, E., Kasen, D., D.Metzger, B., Elias, J., Briceno, C., D.Alexander, K., K.Blanchard, P., *et al.*, 2017, *ApJ.Lett.*, **848**, 18 [[arXiv:1710.05456](#)].

Nynka, M., Ruan, J.J., Haggard, D., (2018) [arXiv:1805.04093](#)

Oates, S.R., Barthelmy, S.D., Baumgartner, W.H., Beardmore, A.P., Evans, P.A., Gehrels, N., Holland, S.T., Kennea, *et al.*, J.A., (2009) *GCN Circ.* **10148**.

Pian, E., D'Avanzo, P., Benetti, S., Branchesi, M., Brocato, E., Campana, S., Cappellaro, E., Covino, S., *et al.*, 2017, *Nature*, **551**, 67 [[arXiv:1710.05858](#)].

Piro, L., Troja, E., Gendre, B., Ghisellini, G., Ricci, R., Bannister, K., Fiore, F., Kidd, L.A., *et al.*, 2014, *ApJ.Lett.*, **790**, 15 [[arXiv:1405.2897](#)].

Predehl, P., Schmitt, J.H.M.M., 1995, *A&A*, **293**, 889.

Pozanenko, A., Barkov, M.V., Minaev, P.Y., Volnova, A.A., Mazaeva, E.D., Moskvitin, A.S., Krugov, M.A., Samodurov, *et al.* V.A., (2017) [[arXiv:1710.05448](#)].

Reina, C., Tarenghi, M., 1973, *A&A*, **26**, 257.

Roming, P.W.A., Koch, T.S., Oates, S.R., Porterfield, B.L., Vanden Berk, D.E., Boyd, P.T., Holland, S.T., Hoversten, E.A., *et al.*, 2009, *ApJ.*, **690**, 163 [[arXiv:0809.4193](#)], Version 2.

Rybicki, G.B., Lightman, A.P., 2004, "Radiative Processes in Astrophysics", Wiele-VCH verlag GmbH & Co.KGaA, Weinheim.

Sari, R., Piran, T., 1995, *ApJ.*, **455**, L143 [astro-ph/9508081](#).

Sari, R., Narayan, R., Piran, T., 1996, *ApJ.*, **473**, 204 [astro-ph/9605005](#).

Savchenko, V., Ferrigno, C., Kuulkers, E., Bazzano, A., Bozzo, E., Brandt, S., Chenevez, J., Courvoisier, T.J.-L., *et al.*, 2017, *ApJ.Lett.*, **848**, L15 [[arXiv:1710.05449](#)].

Slane P., in "Handbook of Supernovae" (2017), 2159, Eds. A.W. Alsabti, P. Murdin, Springer, Cham [[arXiv:1703.09311](#)].

Smartt, S.J., Chen, T.W., Jerkstrand, A., Coughlin, M., Kankare, E., Sim, S.A., Fraser, M., Inserra, C., *et al.*, 2017, *Nature*, **551**, 75 [[arXiv:1710.05841](#)].

Soares-Santos, M., Holz, D.E., Annis, J., Chornock, R., Herner, K., Berger, E., Brout, D., Chen, H., *et al.*, 2017, *ApJ.Lett.*, **848**, L16 [[arXiv:1710.05459](#)].

Tanabashi, M., *et al.*, 2018, *Phys. Rev. D*, **98**, 030001 ([Particle Data Group](#)).

Tanvir, N.R., Levan, A.J., Fruchter, A.S., Hjorth, J., Hounsell, R.A., Wiersema, K., Tunnicliffe, R., 2013, *Nature*, **500**, 547 [[arXiv:1306.4971](#)].

Tchekhovskoy, A., McKinney, J.C., Narayan, R., 2008, *MNRAS*, **388**, 1365 [[arXiv:0803.3807](#)].

Troja, E., Piro, L., van Eerten, H., Wollaeger, R.T., Im, M., Fox, O.D., Butler, N.R., Cenko, S.B., *et al.*, 2017, *Nature*, **551**, 71 [[arXiv:1710.05433](#)].

Troja, E., Piro, L., Ryan, G., van Eerten, H., Ricci, R., Wieringa, M., Lotti, S., Sakamoto, T., Cenko, S.B., (2018) [[arXiv:1801.06516](#)].

Villar, V.A., Cowperthwaite, P.S., Berger, E., Blanchard, P.K., Gomez, S., Alexander, K.D., Margutti, R., Chornock, R., *et al.*, (2018) [[arXiv:1805.08192](#)].

Donald C. Warren, Donald C. Ellison, Maxim V. Barkov, Shigehiro Nagataki 2017, *ApJ.*, **835**, 248 [[arXiv:1701.04170](#)].

Ziaeepour, H., 2009, *MNRAS*, **397**, 361 [[arXiv:0812.3277](#)].

Ziaeepour, H., Gardner, B., 2011, *J. Cosmol. Astrop. Phys.*, **12**, 001 [[arXiv:1101.3909](#)].

Ziaeepour H., 2018, *MNRAS*, **478**, 3233 [[arXiv:1801.06124](#)].